Residual activity induced by heavy ions and beam-loss criteria for heavy-ion accelerators

I. Strašík,[1] E. Mustafin,[1] and M. Pavlovič[2]

[1]*GSI Helmholtzzentrum für Schwerionenforschung Darmstadt, Planckstrasse 1, D64291 Darmstadt, Germany*
[2]*FEI STU, Ilkovičova 3, SK-81219 Bratislava, Slovak Republic*

(Received 2 February 2010; published 28 July 2010)

The paper presents results of FLUKA simulations of the residual activity induced by heavy ions in two target configurations representing: (1) a beam pipe of an accelerator and (2) a bulky accelerator structure like a magnet yoke or a coil. The target materials were stainless steel and copper representing the most common construction materials used for basic accelerator components. For these two materials, the inventory of the induced isotopes depends mainly on the target material and much less on the projectile species. Time evolution of the induced activity can be described by means of a generic curve that is independent from the projectile mass. Dependence of the induced residual activity on selected ion beam parameters was studied. The main goal of the study was establishing a scaling law expanding the existing proton beam-loss tolerance to heavy-ion beams. This scaling law enables specifying beam-loss criteria for projectile species from proton up to uranium at energies from 200 MeV/u up to 1 GeV/u.

DOI: 10.1103/PhysRevSTAB.13.071004 PACS numbers: 29.20.−c, 24.10.Lx, 61.80.Jh, 25.70.Mn

I. INTRODUCTION

Activation of accelerator components due to beam losses during normal machine operation is an important issue especially for high-energy hadron accelerators [1–3]. The residual activity induced by lost beam particles is a dominant source of exposure to personnel and one of the main access restrictions for ''hands-on'' maintenance [1,4]. In addition to this, beam losses may cause damage or reduce lifetime of radiation-sensitive components of the accelerator [5,6].

The activation process consists of various types of nuclear interactions. The most important interactions are high-energy inelastic hadron interactions (spallation reactions), neutron radiative capture, and photonuclear reactions [2]. The radioactive nuclides are produced by primary ions (projectiles) as well as by secondary particles such as protons, neutrons, and fragments generated by interaction of the primary beam with the target material [1]. Activation by the secondary particles is a dominating mechanism for heavy-ion beams, which is experimentally manifested by its presence far beyond the range of the primary particles [7–10]. On top of that, the heavy projectiles are fragmented into radioactive projectile fragments that remain implanted in the target. However, their contribution to the total residual activity is negligible for high-energy heavy-ion projectiles [8–10].

Generally, the induced residual activity depends on the amount, energy, and mass of the lost particles as well as on the composition of the irradiated material [1]. It was shown earlier that the induced residual activity decreases with increasing primary-ion mass [11–13] and with decreasing energy [13]. Quantification of the residual activity provides fundamental information that can be used in several ways: (1) to specify the tolerable beam losses in the machine, (2) to optimize the choice of construction materials, or (3) to estimate the necessary ''cooling'' time after turning off the beam. All these three measures are important with respect to the reduction of personnel exposure.

In the frame of the FAIR project (Facility for Antiproton and Ion Research) [14,15] extensive experimental studies [8–10] and Monte Carlo simulations [12,13,16] of the residual activity induced by high-energy heavy ions in copper and stainless steel were performed at GSI Helmholtzzentrum für Schwerionenforschung in Darmstadt. The presented results of the simulations by FLUKA [17,18] follow the previous residual activation studies [11–13] and give a more elaborated beam-loss criterion for heavy-ion accelerators.

II. CRITERION FOR HIGH-ENERGY PROTON ACCELERATORS

The only available information is the experience that activation caused by uncontrolled beam losses uniformly distributed along the beam line of 1 W/m can be accepted for high-energy proton accelerators as a threshold for the ''hands-on'' maintenance [4]. The beam power of 1 W is equivalent, for example, to 6.24×10^9 protons/s at 1 GeV. In order to quantify the activation caused by 1 W/m of proton-beam losses, the FLUKA code version 2008.3.6 was used to calculate the effective-dose rate in the vicinity of a beam pipe irradiated by 1 GeV protons. The beam particles were distributed uniformly along the beam line as shown in Fig. 1.

In the FLUKA simulation, the new evaporation model with heavy-fragment evaporation was used. Emission of the high-energy light fragments through the coalescence mechanism was activated. The heavy-ion transport with nuclear interactions was switched on. Low-energy neutron transport was simulated down to thermal energies

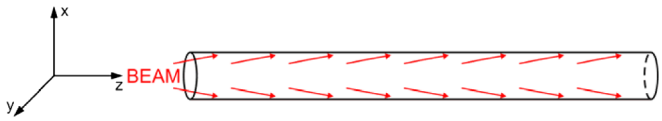

FIG. 1. (Color) A model of the beam-pipe irradiation. X and Y axes are horizontal and vertical axes, respectively, and the Z axis coincides with the beam-pipe longitudinal axis that coincides with the beam axis. The beam propagates in the Z direction.

(10^{-5} eV) and residual nuclei from low-energy neutron interactions were scored.

The assumed beam-pipe geometry was a 10 m long tube made of stainless steel, 10 cm inner diameter, 2 mm wall thickness. The assumed stainless-steel composition was C (0.07%), Mn (2.0%), Si (1.0%), Cr (18%), Ni (9.5%), and S (0.03%) in addition to iron (stainless steel 304). The glancing angle between the incident beam particles and the inner surface of the beam pipe was 1 mrad. The irradiation time was 100 days. The effective-dose rate was calculated 4 hours after the end of irradiation. These conditions were agreed in the accelerator community as representing a typical operating period of an accelerator followed by a reasonable ''cooling down'' time before the ''hands-on'' maintenance [19]. Figure 2 shows the calculated effective-dose rate map in the vicinity of the beam pipe in the horizontal XY plane ($Y = 0$). The effective-dose rate in the XY plane at $Z = 500$ cm at the distance of 30 cm from the surface of the tube is 1.1 mSv/h, which is well consistent with previous activation studies using other simulation codes [19–24].

The knowledge that the effective-dose rate level in the vicinity of the accelerator is around 1 mSv/h is important from the legal radiation protection point of view. If the ambient dose-equivalent rate, which is according to International Commission on Radiation Units & Measurements a conservative estimate of the effective-dose rate, is below 1 mSv/h, the High Radiation Area classification according to the U.S. radiation regulations is avoided [25]. According to German Radiation Protection Ordinance [26], areas with the ambient dose-equivalent rate below 3 mSv/h are classified as Radiation Controlled Areas and ''hands-on'' maintenance is still allowed under specially defined conditions.

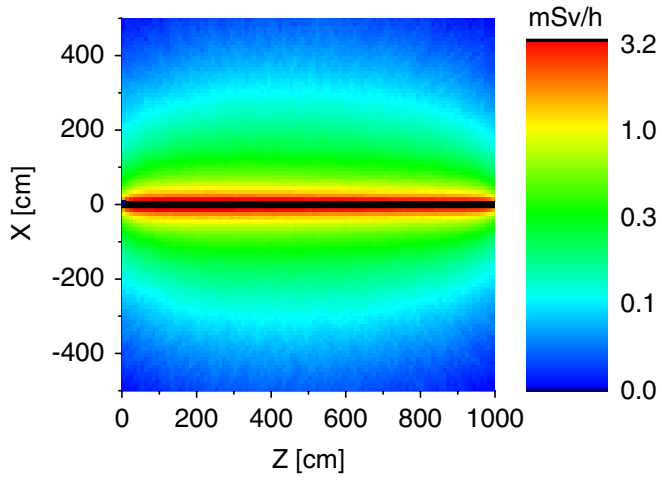

FIG. 2. (Color) Effective-dose rate map in the vicinity of the beam pipe in the horizontal XZ plane ($Y = 0$ cm).

III. BEAM-LOSS CRITERION FOR HEAVY-ION ACCELERATORS

A. Inventory of the isotopes induced in the beam pipe of an accelerator

FLUKA 2008.3.6 was used for simulation of the residual activity induced by various projectiles in the stainless-steel (the same type as above) beam pipe in order to compare heavy ions with protons. In the simulations, the same physical models as described in Chapter II were used. The simulations were performed for ^{1}H, ^{4}He, ^{12}C, ^{20}Ne, ^{40}Ar, ^{84}Kr, ^{132}Xe, ^{197}Au, and ^{238}U at energies from 200 MeV/u up to 1 GeV/u. The simulated irradiation time was 100 days. The residual activity and the effective-dose rate at the distance of 30 cm from the beam-pipe outer surface were calculated at different time points during and after irradiation.

It was found that the inventory of isotopes with a dominating contribution to the total activity as well as their relative activities (relative with respect to the total activity) do not depend strongly on the projectile species (see Fig. 3). This can be explained by the fact that the isotopes are produced mostly by secondary particles rather than by the primary projectiles, as confirmed also experimentally [8–10].

B. Time evolution of the activity

Since the inventory of the isotopes and their relative activities are very similar for all projectiles, the time

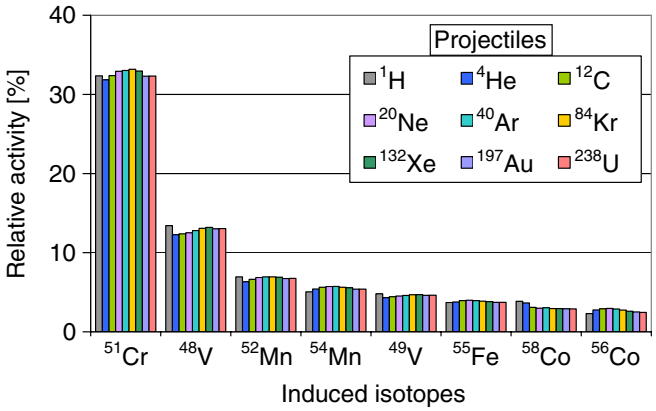

FIG. 3. (Color) Relative activities of the isotopes induced by 1 GeV/u projectiles from proton up to uranium in the stainless steel beam pipe 1 day after the end of irradiation. The relative standard uncertainty of the calculated activities ranged from 0.19% (high-activity isotopes) to 1.17% (low-activity isotopes).

evolution of the activity can be described by means of a generic curve that can be made independent from the projectile mass. In order to do so, the activities must be first normalized to the activity at a certain specific time point, most conveniently at the end of irradiation. The generic curve is then obtained by averaging the data points of the individual curves corresponding to different primary ions. As an example, the time-evolution curves for projectiles at 500 MeV/u calculated for 100 days of continuous irradiation and followed up during 400 days after the end of irradiation is shown in Fig. 4 together with the corresponding generic curve. The largest deviation of individual data points from the generic curve is less than 12%.

Mathematically speaking, the data points of the generic curve (GC) are constructed as

$$A_{\mathrm{GC}} = \langle {}^{j}A \rangle, \tag{1}$$

where A_{GC} is the activity given by the generic curve at a certain time point and ${}^{j}A$ is the activity induced by the jth projectile at the same time point. The activities are normalized to the activity at the end of irradiation.

The generic curve can be obviously divided into two separate parts corresponding to: (1) activation—data points before the end of irradiation and (2) decay—data points after the end of irradiation. Fitting the generic curve is only possible using two different functions for the activation and the decay part, respectively.

A real activation curve is given as

$$A(t_a) = \sum_{i=1}^{N} g_i \left[1 - \exp\left(-\frac{\ln 2}{T_i} t_a \right) \right], \tag{2}$$

where $A(t_a)$ is the total activity at the time t_a after the start of irradiation, g_i are the production rates of the individual isotopes, T_i are the corresponding half-lives, and N is the total number of induced isotopes.

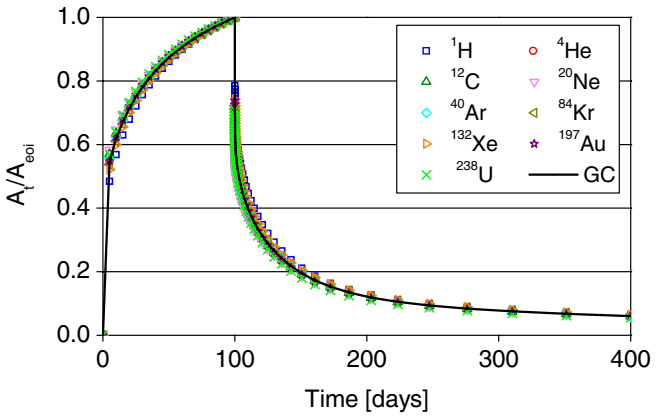

FIG. 4. (Color) Time evolution of the relative activity induced in the beam pipe by different projectiles at 500 MeV/u. A_t is the induced activity as a function of time; A_{eoi} is the induced activity at the end of irradiation. The generic curve (GC) is obtained by averaging the data points of the individual curves corresponding to different primary ions. The relative standard uncertainty of the presented data points is less than 0.85%.

Similarly, a real decay curve is described as follows:

$$A(t_d) = \sum_{i=1}^{N} A_i \exp\left(-\frac{\ln 2}{T_i} t_d \right), \tag{3}$$

where $A(t_d)$ is the total activity at the time t_d after the end of irradiation, A_i are the activities of the individual isotopes at the end of irradiation, T_i are the corresponding half-lives, and N is the total number of induced isotopes. It should be noted that Eqs. (2) and (3) are exactly valid only if all isotopes are produced exclusively by an ion-irradiation mechanism without contribution from daughter products. This assumption is not completely true in reality, but it is justified by the experimental studies when the residual activity was followed up in several time points after the end of irradiation and no significant deviations from the exponential decay law were observed [8–10]. This indicates that the contribution from the daughter products can be neglected in comparison with the activity of the isotopes produced directly by the ion-irradiation mechanism.

For the above reasons, we looked for a possible fit of the activation part of the generic curve by a function formally equivalent to Eq. (2) with $N = 3$ and free parameters g_i and T_i being a result of the fit. Three terms were sufficient to obtain a satisfactory fit with the following parameters: $g_1 = 0.473 \pm 0.002$, $g_2 = 0.156 \pm 0.006$, $g_3 = 0.490 \pm 0.003$, $T_1 = 0.852 \pm 0.019$ d, $T_2 = 9.32 \pm 0.40$ d, and $T_3 = 48.8 \pm 1.4$ d. χ^2_{red} (reduced Chi square) and R^2_{adj} (adjusted R square) parameters indicating the fit quality are 0.97 and 1.00, respectively.

Fitting the decay part of the generic curve was done by a function formally equivalent to Eq. (3) with $N = 5$. The higher number of terms for the decay part was chosen because of longer cooling time compared with the irradiation time. The parameters of the fit are: $A_1 = 0.306 \pm 0.007$, $A_2 = 0.111 \pm 0.004$, $A_3 = 0.126 \pm 0.004$, $A_4 = 0.332 \pm 0.003$, $A_5 = 0.125 \pm 0.002$, $T_1 = 0.0163 \pm 0.0009$ d, $T_2 = 0.214 \pm 0.018$ d, $T_3 = 3.80 \pm 0.22$ d, $T_4 = 25.9 \pm 0.4$ d, and $T_5 = 281 \pm 7$ d. χ^2_{red} and R^2_{adj} parameters are 0.99 and 1.00, respectively. The fitting was performed with the ORIGIN code.

C. Dependence of the residual activity on selected beam parameters

Dependence of the residual activity induced in the beam pipe by 1 W/m of primary beam-loss on ion mass is shown in Fig. 5 for 1 GeV/u and 200 MeV/u beams. The residual activity was calculated at several time points after the end of irradiation: immediately, 1 day, 1 week, 2 months, 1 year, and 10 years. It can be seen that the induced activity is decreasing with increasing ion mass. It is also decreasing

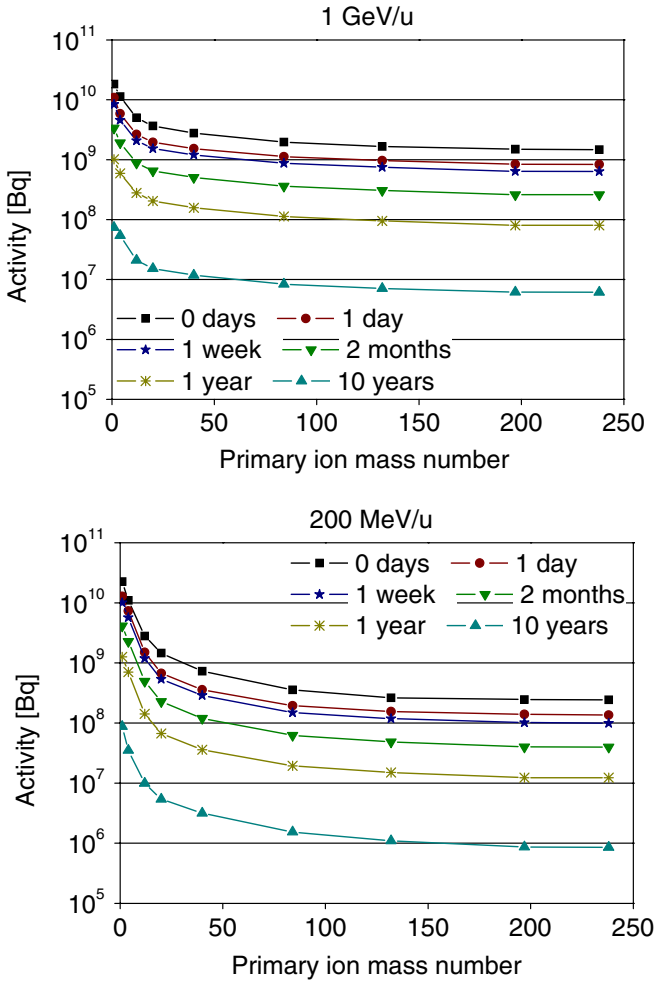

FIG. 5. (Color) Activity of the stainless-steel beam pipe induced by 1 W/m of primary beam loss at 1 GeV/u (upper) and 200 MeV/u (lower). The relative standard uncertainty of the data points ranges from 0.05% to 0.66%.

with decreasing energy. The same trend was observed for the effective-dose rate.

The decrease of the activity with increasing ion mass as well as decreasing ion energy can be explained by the fact that the primary ions at lower energies and with higher mass number are stopped mostly by Coulomb interaction with the target electrons and only a minor part of them interacts with the target nuclei. In other words, the Coulomb stopping range of these particles is shorter compared to their mean-free path for nuclear interaction. In contrary, protons and light ions have their ranges longer than the mean-free path (see Fig. 6). The range to mean-free-path ratio translates into the probability of nuclear interaction that is essentially different for light and heavy ions. For example, the probability of nuclear interaction for protons and ^{4}He ions at 1 GeV/u is almost 100%, which means that almost all beam particles interact with the target nuclei. For ^{238}U ions at 1 GeV/u, the probability of nuclear interaction is only about 50% [13].

The mean-free path, λ, and the nuclear interaction probability, P, can be calculated using the formulas from Refs. [11,27]:

$$\lambda = \frac{A_t}{\rho N_A \sigma_{\mathrm{tot}}}, \tag{4}$$

where A_t is the mass number of the target material, ρ is the density of the target material, N_A is the Avogadro constant, and σ_{tot} is the total cross section of nuclear interaction:

$$\sigma_{\mathrm{tot}} = \frac{\sum_i \sigma_i n_i}{\sum_i n_i}, \tag{5}$$

where σ_i is the cross section for nuclear interaction for given element and n_i is its concentration in the target material. The cross section σ_i can be expressed as [27]

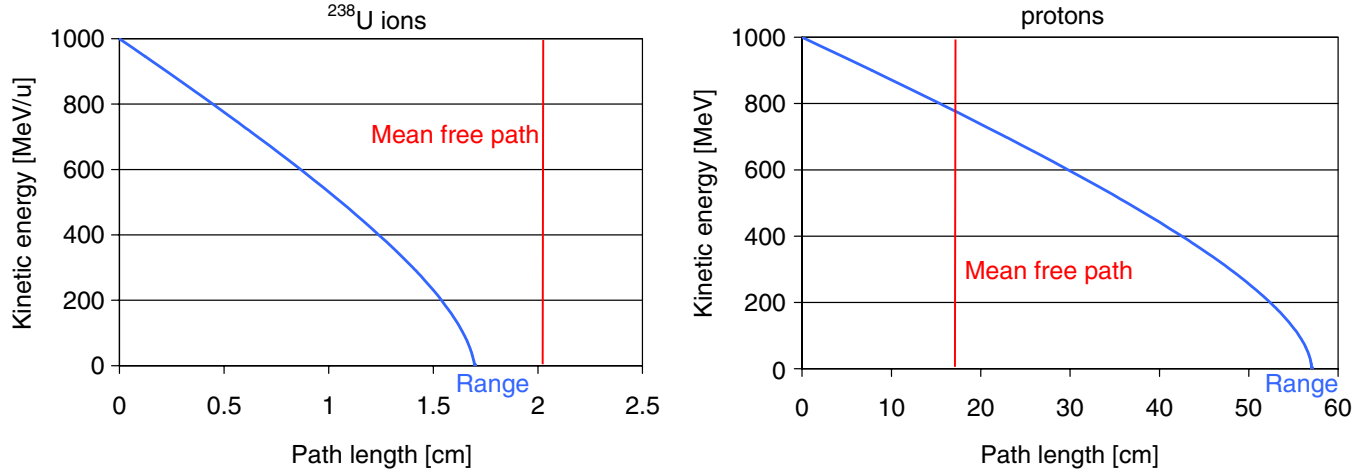

FIG. 6. (Color) Comparison of the Coulomb stopping range and the mean-free path for nuclear interaction of 1 GeV/u ^{238}U ions and protons in stainless steel. The range was calculated by the SRIM code [36]. The mean-free path was calculated as explained below.

$$\sigma_i = \pi r_0^2 \left(A_t^{1/3} + A_p^{1/3} + a \frac{A_t^{1/3} A_p^{1/3}}{A_t^{1/3} + A_p^{1/3}} - c \right) \left(1 - \frac{B_C}{E_K} \right), \quad (6)$$

where $r_0 = 1.1 \times 10^{-15}$ m, $a = 1.85$, A_t and A_p are the mass numbers of the target material and the primary ion, respectively, parameter c depends on energy, however we can assume a constant $c = 2$ in the energy region from 100 MeV/u to 1 GeV/u with accuracy of about 10%. E_K is the kinetic energy of the primary ion and B_C is the Coulomb barrier.

The probability of nuclear interaction, P, is then given by the relation

$$P = 1 - \exp\left(-\frac{R}{\lambda} \right), \quad (7)$$

where R is the range.

D. Scaling law for beam-loss tolerance

So far, it was found out that: (1) inventory of the isotopes induced in the stainless-steel beam pipe does not depend strongly on the projectile species, (2) time evolution of the induced activity correlates to the generic curve, and (3) the activity induced by 1 W/m of beam losses is decreasing with increasing ion mass and with decreasing energy. These facts allow us to introduce a scaling law for heavy-ion beam-loss tolerances based on the accepted criterion of 1 W/m for protons. For this purpose, we define the *normalized activity* as the activity induced by unit beam power of 1 W representing the lost beam particles hitting the accelerator structures. In the case of the beam-pipe geometry, these lost beam particles are assumed to be distributed uniformly along the beam pipe. The scaling factor is then obtained as the ratio of the normalized activity induced by 1 GeV proton (reference) beam to the normalized activity induced by the beam of interest. Although the normalized activity induced by 1 GeV protons is slightly different from the normalized activity induced by protons at lower energy, 1 GeV protons were taken as a reference in order to get a universal criterion.

Simulations of the beam-pipe activation showed that normalized activity induced by uranium ions is about 12 times lower at 1 GeV/u, 23 times lower at 500 MeV/u, and almost 75 times lower at 200 MeV/u compared to 1 GeV protons. Therefore the tolerable beam losses for uranium beam could be 12 W/m at 1 GeV/u, 23 W/m at 500 MeV/u, and 75 W/m at 200 MeV/u. Other particles were treated in the same manner and results are plotted in Fig. 7. The same results were obtained from calculated effective-dose rates.

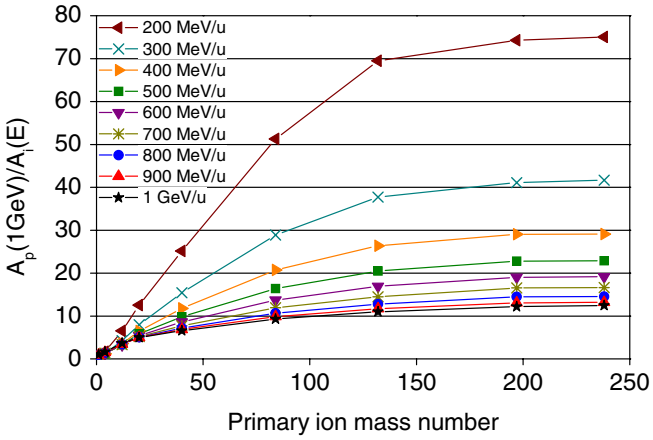

FIG. 7. (Color) Scaling factor for the beam-loss tolerance as a function of primary-ion mass. The scaling factor is represented by the ratio of the normalized activity induced by 1 GeV proton beam, A_p(1 GeV), to the normalized activity induced by the beam of interest at given energy, $A_i(E)$. The activities were calculated by FLUKA at the end of irradiation. The relative standard uncertainty of the presented data is less than 0.76%.

IV. ACTIVATION OF BULKY ACCELERATOR STRUCTURES

A. Simulation model

Besides the beam pipe, accelerators contain also bulky structures like a magnet yoke or a coil. For this reason, FLUKA simulations of the activity induced by various projectiles were performed also for a bulky target. The assumed geometry of the bulky target was a full-material cylinder of 20 cm in diameter, 60 cm long. In this case the beam particles were not distributed uniformly along the target, rather they impacted the basement of the cylinder perpendicularly to its surface (see Fig. 8).

The target materials were stainless steel 304 and copper. The simulations were performed for the same projectiles as for the beam pipe: ^{1}H, ^{4}He, ^{12}C, ^{20}Ne, ^{40}Ar, ^{84}Kr, ^{132}Xe, ^{197}Au, and ^{238}U at energies from 200 MeV/u up to 1 GeV/u. The calculated induced activities were normalized to the unit beam power of 1 W delivered continuously to the target during 3 months. The activity was calculated again at several time points after irradiation: at the end of irradiation, 1 day, 1 week, 2 months, 1 year, and 10 years after the end of irradiation.

FIG. 8. (Color) Geometrical model of the bulky-target irradiation.

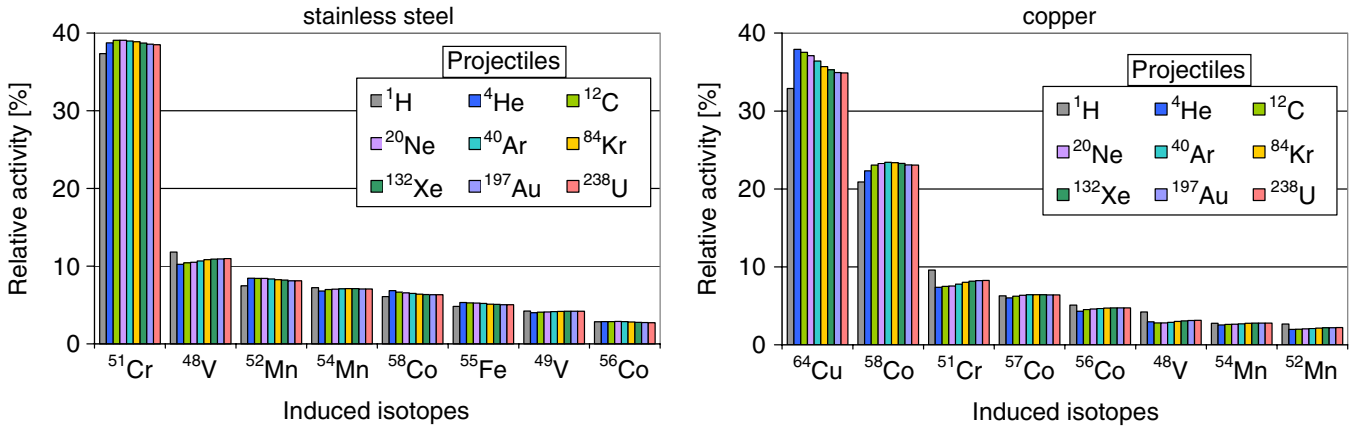

FIG. 9. (Color) Isotope inventory and their relative activities 1 day after the end of irradiation induced by 1 GeV/u projectiles from proton up to uranium in stainless steel and copper bulky target. Relative standard uncertainty of the calculated activity of individual isotopes ranged from 0.12% (high-activity isotopes) to 1.24% (low-activity isotopes).

B. Scaling law for beam-loss tolerance

Similarly to the beam pipe, the inventory of the isotopes induced in the bulky target and their relative activities do not depend strongly on the projectile species, especially for the stainless steel. However, a well-pronounced dependence on the target material was observed (see Fig. 9).

The normalized activity induced in the bulky target is again decreasing with increasing ion mass. For uranium ions, it is about 5 times lower at 1 GeV/u, about 12 times lower at 500 MeV/u, and almost 60 times lower at 200 MeV/u compared to 1 GeV protons. Therefore the tolerable beam losses for uranium beam could be 5 W/m at 1 GeV/u, 12 W/m at 500 MeV/u, and 60 W/m at 200 MeV/u. Other particles were treated in the same manner and results are plotted in Fig. 10 for both materials.

Although the inventory of induced isotopes and their relative activities in stainless steel and copper are different, the ratio of the normalized activity induced by protons to the normalized activity induced by heavy ions is almost the same in both materials. This is due to the fact that both normalized activities (i.e. normalized activity induced by protons as well as by heavy ions) change similarly with the change of the target material, hence keeping the ratio almost constant. For this reason the estimated beam-loss criteria for bulky target are valid for stainless steel as well as for copper.

C. Comparison of the beam-loss criteria for the bulky target and for the beam pipe

It can be seen by comparing Figs. 7 and 10 that the beam-loss criteria for heavy ions are less strict in the case

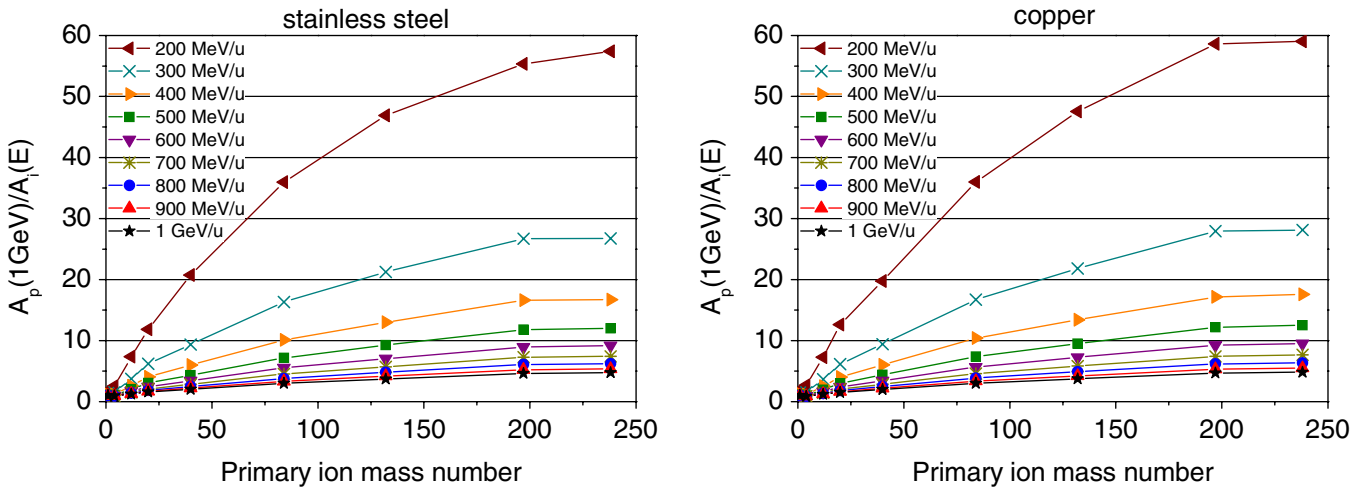

FIG. 10. (Color) Scaling factor for the beam-loss tolerance as a function of ion mass for the bulky target. The scaling factor is represented by the ratio of the normalized activity induced by 1 GeV proton beam, A_p(1 GeV), to the normalized activity induced by the beam of interest at given energy, $A_i(E)$. The activities were calculated by FLUKA at the end of irradiation. The relative standard uncertainty of the presented data is less than 0.89%.

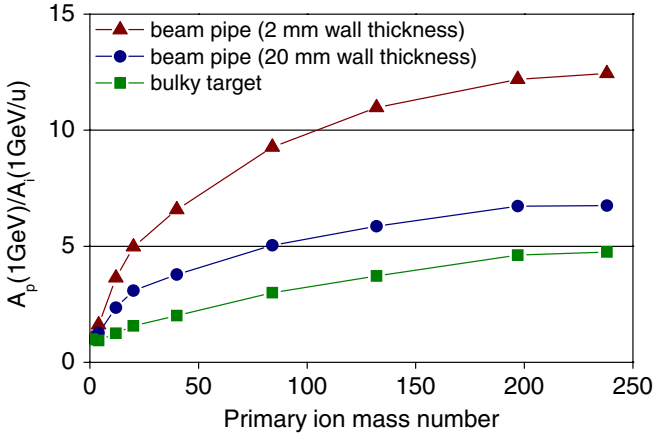

FIG. 11. (Color) Scaling factor for the beam-loss tolerance for the stainless-steel beam pipe with different wall thickness and for the bulky target. The scaling factor is represented by the ratio of the normalized activity induced by 1 GeV proton beam, A_p(1 GeV), to the normalized activity induced by 1 GeV/u ion beam of interest, A_i(1 GeV/u). The activities were calculated by FLUKA at the end of irradiation. The relative standard uncertainty of the presented data is less than 0.78%.

of the beam pipe than in the case of the bulky target. In general, the scaling factor for the beam-loss criteria depends on the target thickness as shown in Fig. 11. The tolerable beam losses for heavy ions decrease with increasing wall thickness.

The physical interpretation of Fig. 11 is based on the knowledge that a major role in the activation process is played by secondary particles, mainly neutrons and protons [8–10]. However, a large number of these nucleons may escape from the target in the case of a thin-wall beam pipe, which lowers the induced activity. The energy spectrum of nucleons emitted from heavy-ion reactions consists of two components: (1) a high-energy component due to the direct (cascade) process and (2) a low-energy component due to the evaporation process. The angular distribution of the cascade nucleons is peaked in the forward direction (from the point of view of initial projectile direction) whereas the evaporated nucleons are emitted nearly isotropically [28]. The direct (cascade) part of the heavy-ion reactions involves projectile breakup and emission of secondary nucleons from the projectile [29,30]. A significant part of the total reaction cross section for heavy-ion collisions belongs to this process. The breakup nucleons with high final energies do not undergo much interaction with the target nuclei and fly away at very forward angles [31]. This allows them to escape from the thin-wall beam pipe. Their contribution to the beam-pipe activation is missing and the induced activity is lower than in the case of the bulky target.

The angular distribution of the nucleons that had escaped from the beam pipe was calculated by FLUKA for two different wall thicknesses. Figure 12 shows the nucleon yield per watt as a function of output angle for the beam-pipe wall thickness of 2 and 20 mm. It can be seen that in the case of the 2 mm thick wall, there is a much higher yield of nucleons leaving the beam pipe at small angles (up to 10 degrees) than in the case of the 20 mm wall. These nucleons must come from the projectiles heavier than protons since they are not observed in the case of proton irradiation. They escape from the thin beam-pipe wall, which lowers the induced activity. It can also be seen that the leakage of the cascade nucleons is significantly reduced in the case of the thicker beam-pipe wall.

V. DISCUSSION

The models used in our simulations as well as the simulation tools contained several simplifications in comparison with the real-life situation. In the progress of our work, further calculations were performed in order to:

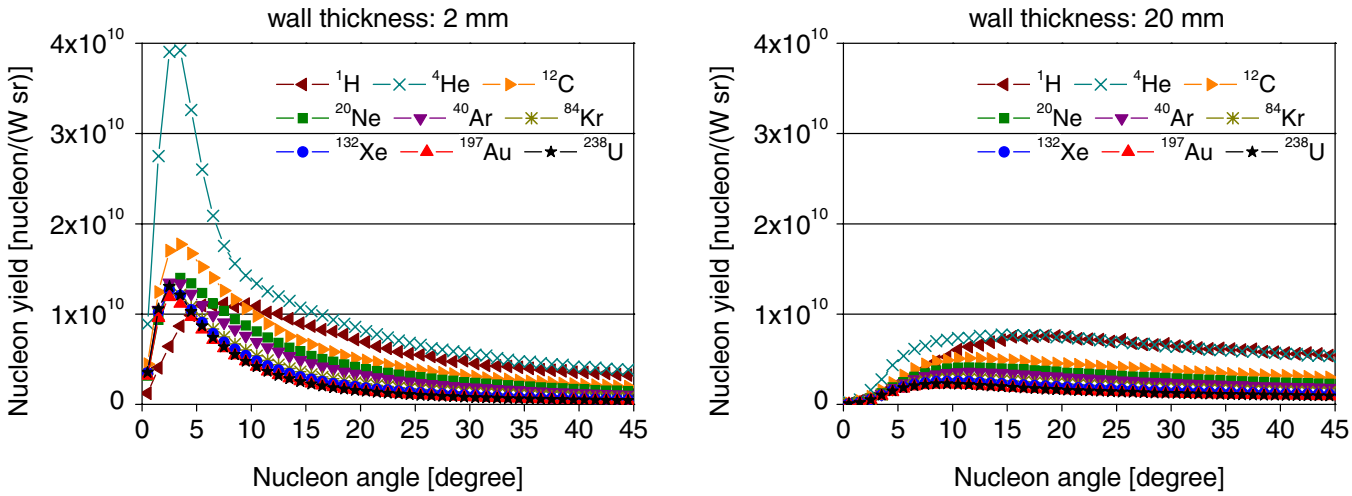

FIG. 12. (Color) Angular distribution of nucleons escaping from the beam pipe for wall thickness of 2 and 20 mm. The angles are given with respect to the beam-pipe longitudinal central axis. The relative standard uncertainty of the presented data is less than 1%.

(a) refine some of the presented results under influence of some model improvements, and/or (b) to study the influence of the model simplifications on the simulation results. These additional calculations are thoroughly described in a dedicated report [32]. In this section, the most important issues and findings are discussed, namely: (a) the impact of the 100 MeV/u interaction threshold of the FLUKA code, (b) the influence of the cobalt containment in the target material, and (c) the influence of the target environment on the activation and beam-loss criteria.

A. Influence of the 100 MeV/u interaction threshold of FLUKA

The influence of the 100 MeV/u interaction threshold of FLUKA was studied by comparing the results of the FLUKA simulations with the results of simulations obtained by means of an independent Monte Carlo particle transport code. We used the SHIELD code [33–35] to calculate residual activity induced in the beam pipe and in the bulky target under the same irradiation conditions as assumed in the FLUKA simulations. The SHIELD code does not cut the inelastic interactions at 100 MeV/u and takes into account production of radioactive nuclides by primary ions with energies down to zero. Results of the SHIELD calculations were processed in the same manner as the FLUKA results and converted into the beam-loss criteria. It was found that, except for 200 MeV/u, the results were very similar. In case of the 200 MeV/u beam energy, the scaling factor based on the FLUKA simulations is higher compared with the scaling factor based on the SHIELD simulations. In terms of the beam-loss criteria, the FLUKA predictions are less strict than the SHIELD predictions. For example, the beam-loss criterion for 200 MeV/u ^{238}U ions based on the FLUKA simulations is 75 W/m, whereas it is 60 W/m when based on the SHIELD simulations. This discrepancy (25%) is very likely caused by the issue of interest—the 100 MeV/u heavy-ion interaction threshold in FLUKA, since the discrepancy between the two codes at higher beam energies is less than 8%.

On the contrary to the beam pipe, there is no such discrepancy between FLUKA and SHIELD at 200 MeV/u in the bulky target. The reason can be that the contribution of activity induced by primary particles compared with the activity induced by secondary particles is higher in the case of the beam pipe than in the case of the bulky target. The leakage of the secondary particles from the beam pipe is higher than the leakage from the bulky target.

B. Influence of the cobalt containment and target environment

Although the target materials of our interest should not contain any cobalt, investigation of the influence of cobalt impurities on residual activity may be relevant for other similar cobalt-containing materials. That is why additional simulations with FLUKA were performed with modified target composition enriched by 1% of cobalt. On top of that, the beam pipe was placed coaxially in a cylindrical concrete tunnel with a wall thickness of 5 m. The distance between the beam pipe and the concrete shielding was 1 m. In the case of the bulky target, the same (1%) cobalt enrichment of the stainless steel was assumed, but the bulky target was surrounded by a spherical concrete shielding with a thickness of 5 m. The distance between the bulky target and the concrete shielding was again 1 m. The calculations with the same concrete shielding were done also for a copper bulky target. For all the above targets, the simulations were performed for protons and ^{238}U ions at 1 GeV/u and 200 MeV/u. The results are presented in Table I. The activities are calculated at the end of irradiation. The spallation products (all inelastic interaction products except for those induced by low-energy neutrons) and low-energy ($E < 20$ MeV) neutron-activation products are scored separately.

It can be seen by analyzing the table data that, in the case of the bare beam pipe without cobalt impurities, the activity of the low-energy neutron-activation products is about a hundred times lower than the activity of the spallation products. In the case of the beam pipe with cobalt impurities and concrete shielding, the activity of the low-energy neutron-activation products does increase by about a factor of 2, but its contribution to the total activity still remains immaterial even after different periods of cooling time [32].

For the bare stainless steel bulky target without cobalt impurities, the activity of the low-energy neutron-activation products is about 10 times lower than the activity of the spallation products. This could be expected since the number of interactions with target material leading to slowing down of the neutrons increases in the bulky target compared with the thin-wall beam pipe. After adding cobalt and shielding, the activity of the low-energy neutron-activation products increases by 25%. However, its contribution to the total activity can be still found of less importance, as checked also by calculations of the activity time evolution [32].

In the last case—the copper bulky target—the activity of the low-energy neutron-activation products is only about 2 times lower than the activity of the spallation products for the nonshielded target (except for 200 MeV protons where it is about 4 times lower). This is caused by the activity of ^{64}Cu ($T_{1/2} = 12.7$ h) that belongs to the isotopes with dominating contribution to the total residual activity shortly after the end of irradiation. The activity of the ^{64}Cu induced by low-energy neutrons is higher than the activity of the ^{64}Cu induced by spallation reactions. With the concrete shielding, the activity of the low-energy neutron-activation products increases roughly by 30%. The difference between the activities of all residual nuclei of the shielded and nonshielded copper bulky target is about 15%. After decay of ^{64}Cu, the activity induced by low-energy neutrons dramatically decreases [32].

TABLE I. Activity induced by protons and ^{238}U ions at 1 GeV/u and 200 MeV/u in different targets. The beam loss is 1 W/m in the case of the beam pipe and 1 W in the case of the bulky target. The activity is calculated at the end of irradiation. Numbers in italic represent relative standard uncertainties.

Activity [Bq]	All residual nuclei	Spallation products	Low-energy neutron-activation products
Stainless-steel beam pipe			
1 GeV protons			
Zero Co containment	1.914×10^{10}	1.897×10^{10}	1.668×10^{8}
No shielding	*0.18%*	*0.18%*	*1.61%*
1% Co containment	1.919×10^{10}	1.890×10^{10}	2.931×10^{8}
Concrete shielding	*0.17%*	*0.17%*	*2.38%*
200 MeV protons			
Zero Co containment	3.304×10^{10}	3.289×10^{10}	1.532×10^{8}
No shielding	*0.32%*	*0.32%*	*3.31%*
1% Co containment	3.302×10^{10}	3.276×10^{10}	2.641×10^{8}
Concrete shielding	*0.30%*	*0.30%*	*4.13%*
1 GeV/u ^{238}U ions			
Zero Co containment	1.557×10^{9}	1.540×10^{9}	1.652×10^{7}
No shielding	*0.05%*	*0.05%*	*0.27%*
1% Co containment	1.566×10^{9}	1.534×10^{9}	3.218×10^{7}
Concrete shielding	*0.06%*	*0.06%*	*0.46%*
200 MeV/u ^{238}U ions			
Zero Co containment	2.885×10^{8}	2.860×10^{8}	2.538×10^{6}
No shielding	*0.22%*	*0.22%*	*1.73%*
1% Co containment	2.903×10^{8}	2.859×10^{8}	4.326×10^{6}
Concrete shielding	*0.22%*	*0.22%*	*2.56%*
Stainless-steel bulky target			
1 GeV protons			
Zero Co containment	4.878×10^{9}	4.470×10^{9}	4.084×10^{8}
No shielding	*0.16%*	*0.17%*	*0.44%*
1% Co containment	5.004×10^{9}	4.466×10^{9}	5.374×10^{8}
Concrete shielding	*0.15%*	*0.15%*	*0.54%*
200 MeV protons			
Zero Co containment	2.718×10^{9}	2.574×10^{9}	1.436×10^{8}
No shielding	*0.40%*	*0.42%*	*1.35%*
1% Co containment	2.786×10^{9}	2.589×10^{9}	1.970×10^{8}
Concrete shielding	*0.39%*	*0.43%*	*1.98%*
1 GeV/u ^{238}U ions			
Zero Co containment	1.041×10^{9}	9.486×10^{8}	9.426×10^{7}
No shielding	*0.07%*	*0.07%*	*0.13%*
1% Co containment	1.075×10^{9}	9.518×10^{8}	1.233×10^{8}
Concrete shielding	*0.06%*	*0.06%*	*0.11%*
200 MeV/u ^{238}U ions			
Zero Co containment	8.895×10^{7}	8.124×10^{7}	7.705×10^{6}
No shielding	*0.31%*	*0.32%*	*0.51%*
1% Co containment	9.253×10^{7}	8.245×10^{7}	1.008×10^{7}
Concrete shielding	*0.28%*	*0.27%*	*0.68%*
Copper bulky target			
1 GeV protons			
Bare bulky target	8.289×10^{9}	5.539×10^{9}	2.751×10^{9}
	0.10%	*0.15%*	*0.41%*
Bulky target with	9.613×10^{9}	5.548×10^{9}	4.065×10^{9}
concrete shielding	*0.13%*	*0.14%*	*0.25%*
200 MeV protons			
Bare bulky target	4.319×10^{9}	3.440×10^{9}	8.796×10^{8}
	0.41%	*0.48%*	*0.77%*
Bulky target with	4.862×10^{9}	3.433×10^{9}	1.429×10^{9}
concrete shielding	*0.35%*	*0.43%*	*0.67%*
1 GeV/u ^{238}U ions			
Bare bulky target	1.746×10^{9}	1.167×10^{9}	5.790×10^{8}
	0.09%	*0.08%*	*0.14%*
Bulky target with	2.030×10^{9}	1.168×10^{9}	8.620×10^{8}
concrete shielding	*0.11%*	*0.10%*	*0.11%*
200 MeV/u ^{238}U ions			
Bare bulky target	1.484×10^{8}	1.029×10^{8}	4.546×10^{7}
	0.40%	*0.36%*	*0.70%*
Bulky target with	1.700×10^{8}	1.025×10^{8}	6.750×10^{7}
concrete shielding	*0.36%*	*0.39%*	*0.68%*

VI. CONCLUSIONS

The beam-loss criteria for high-intensity heavy-ion accelerators were specified for the beam-pipe geometry and the bulky-target geometry. Simulations showed that in the materials of interest (stainless steel and copper), the inventory of the induced isotopes and their relative activities do not depend strongly on the projectile species and energy in the investigated energy-interval from 200 MeV/u up to 1 GeV/u. They depend mainly on the target material. Since the isotopes and their relative activities are very similar for all projectiles, the time evolution of the induced activity correlates to a generic curve. A suitable fit of the general curve was found. The induced activity normalized per unit beam power decreases with increasing primary-ion mass and with decreasing energy. The tolerable beam losses for heavy ions were specified by scaling the existing value of 1 W/m for protons. The scaling yields the beam-loss tolerances for uranium beam of 12 W/m at 1 GeV/u, 23 W/m at 500 MeV/u, and 75 W/m at 200 MeV/u in the case of the beam-pipe geometry. The beam-loss tolerances for the bulky accelerator structures are stricter. They are 5 W/m at 1 GeV/u, 12 W/m at 500 MeV/u, and 60 W/m at 200 MeV/u for uranium beam. The thin-wall beam pipe exhibits significant leakage of the projectiles' breakup nucleons from the wall, which decreases the induced activity.

Furthermore, influence of selected model settings on the simulation results was investigated and the following conclusions can be drawn.

The 100 MeV/u threshold for heavy-ion inelastic interactions in the FLUKA code has only modest impact on the beam-loss criteria. The largest discrepancy of about 25% was observed for low-energy (200 MeV/u) beams and

beam-pipe geometry. In the case of higher energies as well as the bulky targets, the beam-loss criteria calculated by FLUKA and SHIELD are similar. The presence of cobalt in stainless steel (even an exaggerated amount of 1%) and the concrete shielding do not affect significantly the total induced activity. These factors influence mainly the activity of the low-energy neutron-activation products that is lower than the activity of spallation products. That is why the total activity is not affected significantly. The biggest difference (15%) in the total residual activity between shielded and nonshielded targets was recognized in the case of the copper bulky target due to the ^{64}Cu. Since this is a short-lived isotope, this difference is relevant only shortly after the end of irradiation.

ACKNOWLEDGMENTS

This work was partially supported by VEGA 1/0129/09.

[1] A. H. Sullivan, *A Guide to Radiation and Radioactivity Levels Near High Energy Particle Accelerators* (Nuclear Technology Publishing, Ashford, Kent, United Kingdom, 1992), Chap. 4, p. 93.
[2] L. Ulrici, M. Brugger, Th. Otto, and S. Roesler, Nucl. Instrum. Methods Phys. Res., Sect. A **562**, 596 (2006).
[3] E. Mauro and M. Silari, Nucl. Instrum. Methods Phys. Res., Sect. A **605**, 249 (2009).
[4] *Proceedings of the 7th ICFA Mini-Workshop on High Intensity High Brightness Hadron Beams, Wisconsin, USA, 1999*, edited by N. V. Mokhov and W. Chou (Fermi National Accelerator Laboratory, Batavia, Illinois, 2000), p. 3.
[5] A. Smolyakov, E. Mustafin, N. Pyka and P. Spiller, in *Proceedings of the 11th European Particle Accelerator Conference, Genoa, 2008* (EPS-AG, Genoa, Italy, 2008), p. 3602.
[6] A. Plotnikov, E. Mustafin, N. Pyka, and P. Spiller, in Ref. [5], p. 3599.
[7] F. Clapier *et al.*, Radiat. Environ. Biophys. **34**, 213 (1995).
[8] A. Fertman *et al.*, Nucl. Instrum. Methods Phys. Res., Sect. B **260**, 579 (2007).
[9] I. Strašík *et al.*, Nucl. Instrum. Methods Phys. Res., Sect. B **266**, 3443 (2008).
[10] I. Strašík, E. Mustafin, T. Seidl, and M. Pavlovič, Nucl. Instrum. Methods Phys. Res., Sect. B **268**, 573 (2010).
[11] E. Mustafin, I. Hofmann, and H. Weick, Nucl. Instrum. Methods Phys. Res., Sect. A **501**, 553 (2003).
[12] I. Strašík *et al.*, Nuclear Technology **168**, 643 (2009).
[13] I. Strašík *et al.*, in Ref. [5], p. 3551.
[14] W. F. Henning, Nucl. Phys. **A805**, 502c (2008).
[15] P. Spiller and G. Franchetti, Nucl. Instrum. Methods Phys. Res., Sect. A **561**, 305 (2006).
[16] E. Kozlova *et al.*, Nuclear Technology **168**, 747 (2009).
[17] G. Battistoniet *et al.*, in *Proceedings of the Hadronic Shower Simulation Workshop 2006* (Fermilab, Batavia, Illinois, 2007), p. 31.
[18] A. Fasso, A. Ferrari, J. Ranft, and P. R. Sala, Reports No. CERN-2005-10, No. INFN/TC_05/11, and No. SLAC-R-773 (2005).
[19] J. Alonso, in Proceedings of the 7th ICFA Mini-Workshop on High Intensity High Brightness Hadron Beams, Wisconsin, USA, 1999 (Ref. [4]), p. 51.
[20] R. T. Santoro *et al.*, in *Proceedings of the 3rd International American Nuclear Society Topical Meeting on Nuclear Applications of Accelerator Technology AccApp'99, Long Beach, USA, 1999* (American Nuclear Society, La Grange Park, Illinois, 1999), p. 417.
[21] M. M. Fikani and E. J. Pitcher, Trans. Am. Nucl. Soc. J. **79**, 384 (1998).
[22] O. E. Krivosheev and N. V. Mokhov, in Proceedings of the 7th ICFA Mini-Workshop on High Intensity High Brightness Hadron Beams, Wisconsin, USA, 1999 (Ref. [4]), p. 85.
[23] R. M. Ronningen, G. Bollen, and I. Remec, Trans. Am. Nucl. Soc. J. **99**, 597 (2008).
[24] R. M. Ronningen, G. Bollen, and I. Remec, Nuclear Technology **168**, 670 (2009).
[25] U. S. Department of Energy, DOE Standard: DOE-STD-1098-99 Radiological Control, 2004.
[26] M. Palm, Kerntechnik **67**, 8 (2002).
[27] S. Kox *et al.*, Phys. Lett. **159B**, 15 (1985).
[28] T. Katoand and T. Nakamura, Nucl. Instrum. Methods Phys. Res., Sect. A **311**, 548 (1992).
[29] M. Maiti, M. Nandy, S. N. Roy, and P. K. Sarkar, Nucl. Instrum. Methods Phys. Res., Sect. A **556**, 577 (2006).
[30] U. Brosa and W. Krone, Phys. Lett. **105B**, 22 (1981).
[31] A. Bonaccorso and D. M. Brink, Phys. Rev. C **57**, R22 (1998).
[32] I. Strašík, E. Mustafin, M. Pavlovič, and N. Sobolevskiy, GSI Report, GDS-ID: DOC-2010-Jun-23, https://www.gsi.de/documents/DOC-2010-Jun-23-1.pdf.
[33] A. V. Dementyev and N. M. Sobolevsky, Radiation Measurements **30**, 553 (1999).
[34] http://www.inr.ru/shield/.
[35] E. Mustafin *et al.*, Radiat. Eff. Defects Solids **164**, 460 (2009).
[36] J. F. Ziegler, J. P. Biersack, and M. D. Ziegler, *SRIM—The Stopping and Range of Ions in Matter* (Lulu Press Co., Morrisville, NC, 2008).